Exploring global changes in agricultural ammonia emissions and their contribution to nitrogen deposition since 1980

Lei Liu[a,1], Wen Xu[b], Xiankai Lu[c], Buqing Zhong[c], Yixin Guo[d], Xiao Lu[e], Yuanhong Zhao[f], Wei He[g], Songhan Wang[h], Xiuying Zhang[g], Xuejun Liu[b,1], and Peter Vitousek[i]

Edited by Robert Howarth, Cornell University, Ithaca, NY; received December 5, 2021; accepted February 7, 2022 by Editorial Board Member Gregory P. Asner

Global gains in food production over the past decades have been associated with substantial agricultural nitrogen overuse and ammonia emissions, which have caused excessive nitrogen deposition and subsequent damage to the ecosystem health. However, it is unclear which crops or animals have high ammonia emission potential, how these emissions affect the temporal and spatial patterns of nitrogen deposition, and where to target future abatement. Here, we develop a long-term agricultural ammonia emission dataset in nearly recent four decades (1980–2018) and link it with a chemical transport model for an integrated assessment of global nitrogen deposition patterns. We found global agricultural ammonia emissions increased by 78% from 1980 and 2018, in which cropland ammonia emissions increased by 128%, and livestock ammonia emissions increased by 45%. Our analyses demonstrated that three crops (wheat, maize, and rice) and four animals (cattle, chicken, goats, and pigs) accounted for over 70% total ammonia emissions. Global reduced nitrogen deposition increased by 72% between 1980 and 2018 and would account for a larger part of total nitrogen deposition due to the lack of ammonia regulations. Three countries (China, India, and the United States) accounted for 47% of global ammonia emissions, and had substantial nitrogen fertilizer overuse. Nitrogen deposition caused by nitrogen overuse accounted for 10 to 20% of total nitrogen deposition in hotspot regions including China, India, and the United States. Future progress toward reducing nitrogen deposition will be increasingly difficult without reducing agricultural ammonia emissions.

ammonia emissions | nitrogen deposition | nitrogen overuse | agriculture

Significance

Agricultural systems are already major forces of ammonia pollution and environmental degradation. How agricultural ammonia emissions affect the spatio-temporal patterns of nitrogen deposition and where to target future mitigation efforts, remains poorly understood. We develop a substantially complete and coherent agricultural ammonia emissions dataset in nearly recent four decades, and evaluate the relative role of reduced nitrogen in total nitrogen deposition in a spatially explicit way. Global reduced nitrogen deposition has grown rapidly, and will occupy a greater dominant position in total nitrogen deposition without future ammonia regulations. Recognition of agricultural ammonia emissions on nitrogen deposition is critical to formulate effective policies to address ammonia related environmental challenges and protect ecosystems from excessive nitrogen inputs.

In the past half-century, humans have increased the amount of reactive nitrogen (N_r) in the environment more than the amount of any other major element (1). N_r compounds in the atmosphere are mainly controlled by the emissions of nitrogen oxides (NO_x) and ammonia (NH_3) (2); NO_x is mainly from the burning of fossil fuels for energy production and NH_3 is mostly from agricultural sources including volatilized livestock waste and nitrogen (N)-based fertilizers (3, 4). Our analyses of N_r have shifted from how to increase food production to a realization that agricultural intensification adds excess N_r that damages environmental systems and degrades human health. Agriculture is responsible for approximately two-thirds of global N_r pollution (2). These emissions result in excessive N_r deposition in terrestrial and aquatic ecosystems, with adverse feedbacks on human and ecosystem health, water eutrophication, soil acidification, and biological diversity; they increase the risk of irreversible and sudden environmental change (5, 6).

Global crop production has doubled in the recent four decades, while synthetic N fertilizer use has tripled over the same period according to the Food and Agriculture Organization (FAO) of the United Nations. The global average nitrogen use efficiency (NUE) for crop production (NUE refers to the ratio of crop N uptake to applied N fertilizer) has decreased from 0.5 in 1961 to 0.4 in 2010 (7), indicating substantial N_r losses to the environment. Agricultural NH_3 emissions are not regulated in most countries, with the exception of Western Europe (8). Due to substantial overuse of agricultural N and inappropriate management, large amounts of NH_3 are volatilized from agricultural systems, and thereby affect atmospheric chemistry and cause high N_r deposition downwind (9, 10). Asian countries overuse N more than do others. The absolute worst case is China, whose average NUE has decreased from more than 60% in 1961 to 25% in 2010 (7). China has implemented a series of policies to encourage the production and use of synthetic fertilizer in the past three decades (11). In 2010, more than 30% of the global fertilizer consumption was used for China's cultivated land (accounting for only 7% of the global cultivated land area). In India, where fertilizer application has doubled in 20 y, its NUE has decreased from 40% in 1961 to 30% in

Author contributions: L.L. and Xuejun Liu designed research; L.L. performed research; L.L. and W.X. analyzed data; and L.L., Xiankai Lu, B.Z., Y.G., Xiao Lu, Y.Z., W.H., S.W., X.Z., Xuejun Liu, and P.V. wrote the paper.

The authors declare no competing interest.

This article is a PNAS Direct Submission. R.H. is a guest editor invited by the Editorial Board.

[1]To whom correspondence may be addressed. Email: liuleigeo@lzu.edu.cn or liu310@cau.edu.cn.

This article contains supporting information online at http://www.pnas.org/lookup/suppl/doi:10.1073/pnas.2121998119/-/DCSupplemental.

Published March 28, 2022.

2010 (7). Decreasing NUE also occurs in many other countries in the world, making the need to increase agricultural productivity, while at the same time reducing environmental impacts related to the use of N fertilizer, a global challenge.

Sustainably meeting global food demands is one of humanity's grand challenges, and it is crucial to produce sufficient food with less pollution in the near future. However, there have been few attempts to evaluate the effect of agricultural NH_3 emissions on N_r deposition systematically while at the same time identifying where to target proposed solutions. In this study, we aimed to identify a small set of regions, crops, and actions that provide strategic global opportunities to reduce NH_3 emissions and N_r deposition, while delivering food more efficiently from existing farmlands. To determine which interventions may have a high degree of global impact in these categories, we use recently published geospatial data and models to analyze the potential reduction of agricultural NH_3 emission in terms of how effective they will be in mitigating N_r deposition.

Results

Agricultural NH_3 Emissions. To start, we constructed a high-resolution global agricultural NH_3 emission dataset (0.083°) for 1980 to 2018 using recently published geospatial data (4, 12) and long-term statistics from the FAO of the United Nations and considering both N application and livestock waste. We use our estimated cropland and livestock NH_3 emission data in the year 2010 shown here as a case study (Fig. 1). We choose 2010 as a representative year in terms of very detailed spatial information of N fertilizer use and livestock data.

We analyzed 16 major crops (including wheat, maize, rice, soybean, etc.) from the FAO of the United Nations. Global agricultural N application was estimated at 144 Tg N in 2010, of which 68% and 32% came from N fertilizer and manure, respectively. The 16 major crops accounted for 73% of global N application (*SI Appendix*, Fig. S1). With current agricultural management, emission factors of NH_3 in croplands were highest over Asia (20%) and lowest in Europe (13%) and had a global average of 17% (*SI Appendix*, Table S3). Global N application produced 28 Tg N as NH_3 emitted to the atmosphere (Fig. 1*A*), in which wheat, maize, and rice accounted for 68% of cropland NH_3 emissions from the 16 major crops analyzed here (Fig. 1*D*). Three countries (China, India, and the United States) had cropland NH_3 emissions of 16 Tg N, accounting for 61% of cropland NH_3 emissions. These results highlight that cropland NH_3 emissions are not evenly distributed by crops or regions.

Besides crops, we also used the recently published gridded livestock database to calculate livestock NH_3 emissions (12) including 8 major animals (buffalo, cattle, chicken, duck, horse, goat, pig, and sheep) (Fig. 1*D*). We used a bottom-up approach to estimate livestock NH_3 emissions, combining animal numbers and emission factors of animals. Emission factors of NH_3 from animals ranged from 0.23 to 18.40 kg N head^{-1} y^{-1} (*SI Appendix*, Table S3), with high values in cattle (dairy cattle as 18.4 kg N head^{-1} y^{-1} and nondairy cattle as 8.5 kg N head^{-1} y^{-1}), followed by horse, buffaloes, pigs, goats, sheep, chickens, and ducks (0.23–8.70 kg N head^{-1}). Total livestock NH_3 emissions were estimated to be 30 Tg N in 2010 (Fig. 1*B*). Generally, NH_3 emissions differ substantially among animal types. Four animals (cattle, chicken, goats, and pigs) accounted for 90% of livestock NH_3 emissions. This suggests that mitigation measures should give priority to these animals with high NH_3 emission potential.

In summary, NH_3 emissions from livestock and cropland systems were 58 Tg N in 2010 (Fig. 1*E*). China, India, and the United States had total NH_3 emissions as 14.5, 8.9, and 4.1 Tg N, which summed to 27.5 Tg N and accounted for 47% of global NH_3 emissions from livestock and N fertilizer. Our estimates of NH_3 emissions had a consistency in the geospatial patterns of the Emission Database for Global Atmospheric Research (EDGAR) and Community Emissions Data System (CEDS) by country (*SI Appendix*, Fig. S3), and were also close to estimates of regional studies of China (14.5 Tg N in this study vs. 12.6 Tg N in Zhang et al. [9]), the United States (4.1 Tg N in this study vs. 3.9 Tg N in Cao et al. [13]), and Western Europe (3.0 Tg N in this study vs. 3.2 Tg N in European Environment Agency [14]) around 2010. Compared to other emission inventories, we not only estimated the total amounts of agricultural NH_3 emissions, but also estimated NH_3 emissions by each crop and animal, which was critical for understanding which crops or animals had high NH_3 emission potential, and thus helpful for formulating future NH_3 abatement measures.

Regarding trends, global agricultural NH_3 emissions increased by 78% from 1980 to 2018, in which cropland NH_3 emissions increased by 128% (14–32 Tg N y^{-1}) and livestock NH_3 emissions increased by 45% (22–32 Tg N y^{-1}). For the spatial changes, both cropland and livestock NH_3 emissions increased substantially including China, India, the United States, South America, and Africa. The largest increase in NH_3 emissions occurred in China and India (for cropland above 10 kg N ha^{-1} and for livestock 5–10 kg N ha^{-1}), while Western Europe had experienced a decline for both cropland and livestock (0–10 kg N ha^{-1}) (Fig. 2). The decline in agricultural NH_3 emissions in Western Europe were associated with NH_3 emission controls, such as the EU National Emissions Ceilings Directive (15, 16).

Reduced vs. Oxidized N_r Deposition. We calculated the overall status of N_r deposition in the base year 2010, using a state-of-the-art chemistry transport model (GEOS-Chem) to simulate global N_r deposition with our estimates of global agricultural NH_3 emissions, while the nonagricultural NH_3 emissions and NO_x emissions were obtained from the Community Emissions Data System (CEDS) (17). The modeled deposition of reduced N_r (NH_x = ammonia [NH_3] + ammonium [NH_4^+]) and oxidized N_r (NO_y, the sum of all oxidized N_r species) show a general agreement with measurements over regions with intensive monitoring sites (the overall bias was below 10% in *SI Appendix*, Fig. S4).

Global N_r deposition was estimated at 119 Tg N in 2010 (land, 60%; seas, 40%) (Fig. 3). We found, for most countries, above 60% of N_r emissions were deposited to their own lands (Fig. 3*F*). For instance, in China, N_r deposition accounted for 75% of its N_r emissions in 2010 (20.4 Tg N), while the remaining 25% was deposited outside China. The ratio of N_r deposition to emissions ($R_{Dep/Emi}$) in China was close to that in the United States (68%) and Western Europe (71%), while $R_{Dep/Emi}$ was close to or larger than 1 for remote regions (e.g., in Greenland), suggesting these regions can be substantially affected by other countries through atmospheric transports. N_r deposition varied substantially with the highest values in the Eastern China (>40 kg N ha^{-1}) and India (20-40 kg N ha^{-1}), followed by the Eastern United States, Western Europe, Central South America, and Africa around the equator (5–20 kg N

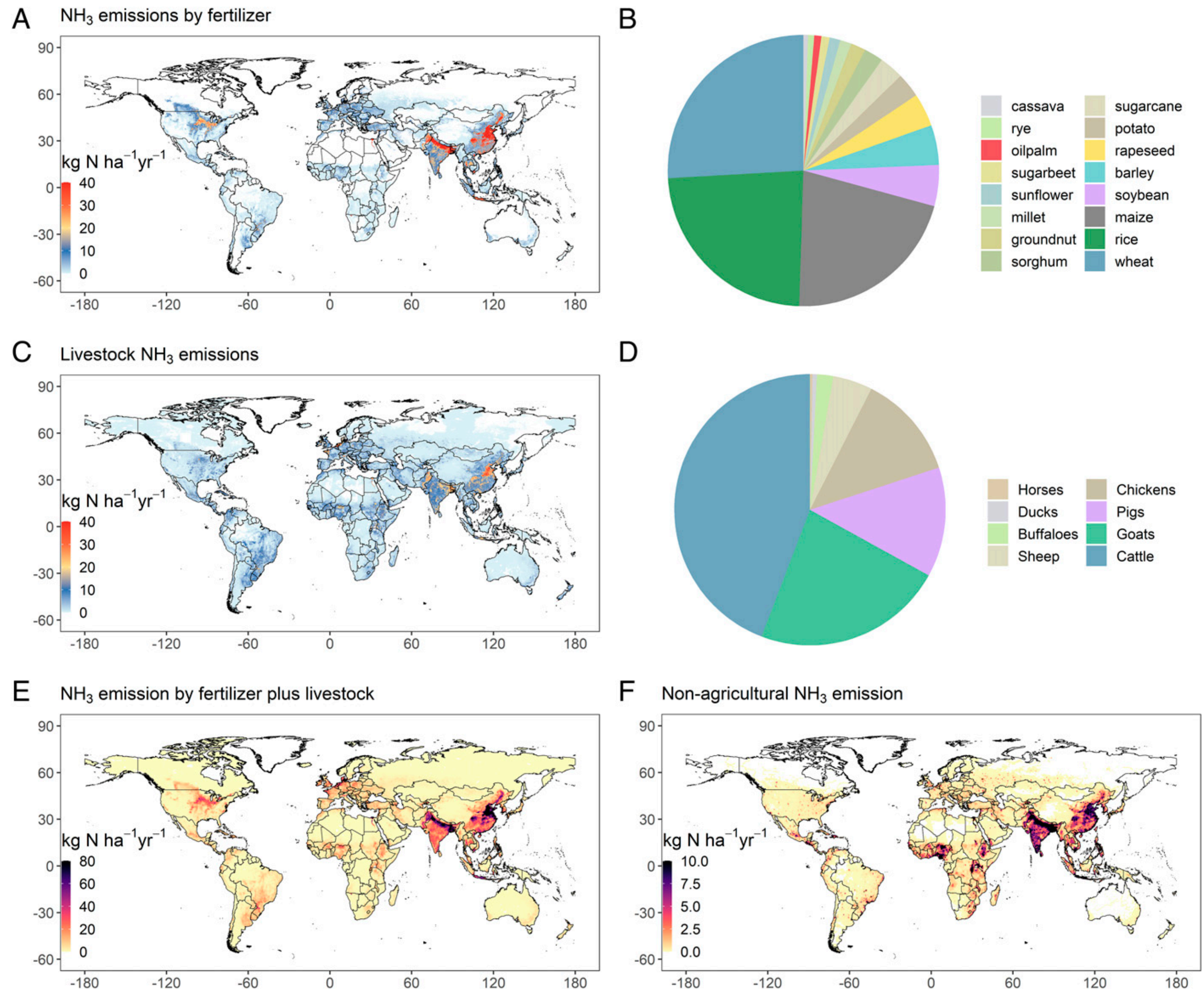

Fig. 1. Agricultural NH_3 emissions in 2010. (*A*) Spatial distribution of cropland NH_3 emissions. (*B*) Contribution of different crops to cropland NH_3 emissions. (*C*) Spatial distribution of NH_3 emissions from livestock. (*D*) Contribution of different animals to livestock NH_3 emissions. (*E*) NH_3 emissions from agriculture (fertilizer plus livestock). (*F*) Nonagricultural NH_3 emissions. The agricultural NH_3 emissions were developed in this study at a high resolution (0.083°), while the nonagricultural NH_3 emissions were based on the Community Emissions Data System (CEDS) NH_3 emissions (0.5°).

ha^{-1}) (Fig. 3*C*). As the world's most polluted region, China's total N_r deposition budgets (15.6 Tg N) in 2010 were approximately three times those over the United States (5.0 Tg N) and Western Europe (4.6 Tg N) in 2010.

NH_x and NO_y deposition showed markedly different spatial patterns (Fig. 3 *A* and *B*). High NO_y deposition mainly appeared in developed regions partly correlated with industrial sources. Instead, high NH_x deposition mainly occurred in

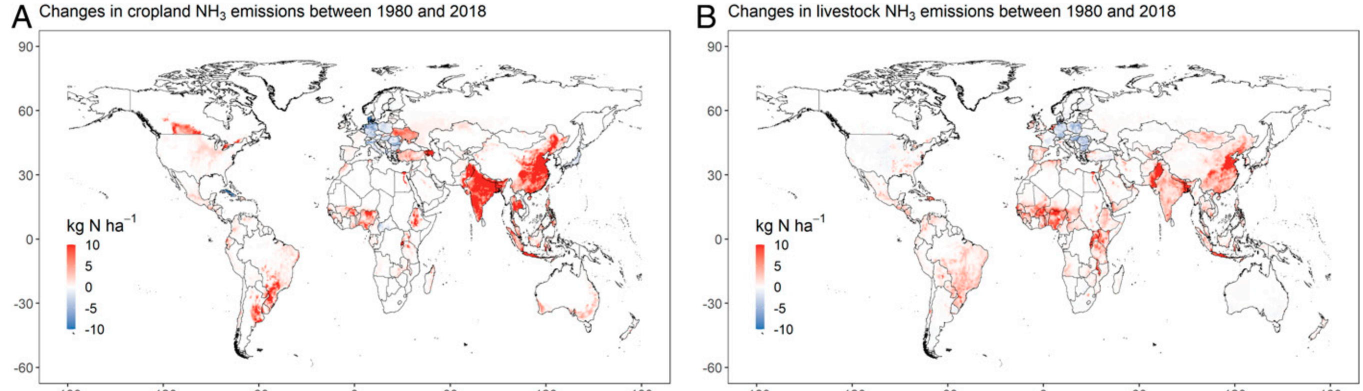

Fig. 2. Changes of (*A*) cropland and (*B*) livestock NH_3 emissions between 1980 and 2018.

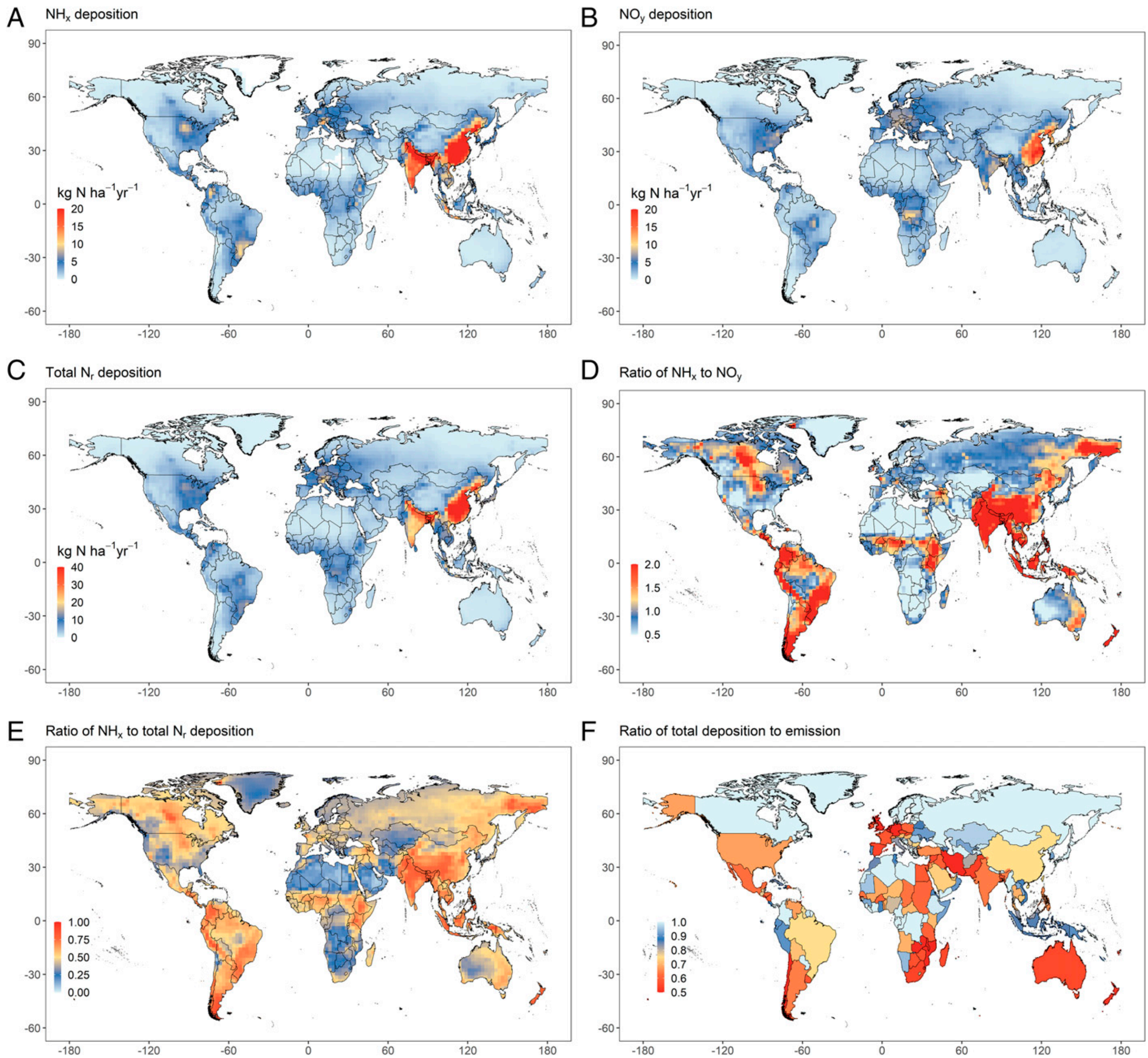

Fig. 3. Atmospheric N_r deposition simulated by the GEOS-Chem model in 2010. (*A–C*) Total NH_x, NO_y, and N_r deposition. (*D*) Gridded ratio of NH_x to NO_y. (*E*) Gridded ratio of NH_x to total N_r deposition. (*F*) Ratio of N_r deposition to N_r emissions. Global agricultural NH_3 emissions between 1980 and 2018 were adopted from our developed high-resolution datasets (at 0.083°), while the nonagricultural NH_3 emissions and NO_x emissions were obtained from the Community Emissions Data System (CEDS).

agricultural regions, which can be evidenced clearly in Eastern China, India and Central Eastern United States. Both NO_y and NH_x deposition exhibited highest (>20 kg N ha^{-1}) over the Eastern China (including North China Plain and Yangtze River Delta Region), with highly developed economy and agriculture (18). High NH_x deposition also occurred in Central South America and Africa around Equator, associated to the large-scale biomass burning (*SI Appendix*, Fig. S6). The ratio of NH_x (NO_y) deposition to NH_3 (NO_x) emissions was also calculated using the GEOS-Chem (*SI Appendix*, Fig. S5). A larger proportion of NH_x was deposited close to the source region, while NO_y could be deposited in more remote regions with atmospheric transports. For instance, the average ratio of deposition to emissions was 82% for NH_x in China, which was higher than that (68%) for NO_y; similar phenomena can be also found in the United States (71% for NH_x and 65% for NO_y), India (68% for NH_x and 55% for NO_y), and Brazil (81% for NH_x and 67% for NO_y).

Fig. 3*D* shows the ratio of NH_x to NO_y deposition ($R_{NHx/NOy}$) globally. $R_{NHx/NOy}$ >1 represented that agriculture was the major source; otherwise fossil fuel combustion was the dominating source (19). As shown in Fig. 3 *D* and *E*, NH_x exceeded NO_y deposition in agricultural regions including the Eastern United States, India, China, and biomass burning regions (Central South America and Africa around the equator), while the Middle East, North Africa, and Greenland were dominated by NO_y deposition. The Greenland had near-zero NO_x and NH_3 emissions, but received more NO_y deposition than NH_x, reflecting that NO_y can be deposited in nearly human untouched areas with a longer transport than NH_x. India's NH_x deposition was approximately triple that of the NO_y deposition (Fig. 3*D*), showing N_r deposition was mainly dominated by NH_x. Over China, the $R_{NHx/NOy}$ was 1.7, indicating NH_x deposition was 70% higher than NO_y deposition. Over Western Europe and the United States, the $R_{NHx/NOy}$ was around 0.8, showing its NH_x deposition was slightly lower than NO_y deposition.

Trends in Reduced and Oxidized N_r Deposition. We constructed the comprehensive long-term oxidized and reduced N_r deposition over the period 1980 to 2018 using the GEOS-Chem model with the high-resolution agricultural NH_3 emissions and CEDS NO_x emissions. For the overlap time period (year 2010) between this study and Tan et al. (20), our estimates of NH_x (63 Tg N) and NO_y (56 Tg N) deposition were close to theirs (NH_x 64 Tg N and NO_y 59 Tg N). The major difference between the two studies was due to the different emission datasets used. We used our developed high-resolution NH_3 emission data and the CEDS NO_x emissions overwritten by several comprehensive regional emission data, while they mainly adopted the EDGAR emissions. Our results show similar estimates with regional studies at corresponding years conducted, such as in China [16.4 Tg N by Zhao et al. (21) vs. 15.6 Tg N in this study during 2008–2010], the United States [6.7 Tg N by Zhang et al. (10) vs. 5.9 Tg N in this study during 2006–2008], and Western Europe [5.1 Tg N by Tan et al. (20) vs. 4.6 Tg N in this study in 2010]. This study provides a robust estimation of global N_r deposition in recent four decades with a consistent and reproducible methodology.

Regarding NO_y deposition trends (Fig. 4 *B* and *C*), the United States and Western Europe have reduced by half (50–60%) due to effective regulations (such as the Clean Air Act) (22) designed to decrease NO_x emissions between 1980 and 2018. NO_y deposition in the United States and Western Europe reached the same low level in 2018 (2.4 vs. 2.4 Tg N). For some countries in Western Europe, the reduction of NO_y deposition even exceeded 60% between 1980 and 2018, for instance in France (67%) and Netherlands (70%) (*SI Appendix*, Fig. S7). In contrast, China has experienced explosive growth of NO_y deposition and increased by more than 5 times from 1980 (1.2 Tg N) to 2012 (6.2 Tg N). Fortunately, China's NO_y deposition has declined by 16% between 2012 and 2018 due to the adoption of emission control technologies for large combustion plants and boilers (23). The decrease in China's NO_y deposition since 2012 was consistent with an observational study (24) based on the Chinese National N_r Deposition Monitoring Network (NNDMN). Although great efforts have been made to reduce NO_x emissions, China still faced a high level of NO_y deposition (5.2 Tg N), which was more double that in the United States and Western Europe in 2018. Global NO_y deposition on land has increased by 40% from 1980 (27 Tg N) to 2016 (38 Tg N), after then it has declined by 16% to 2018 (32 Tg N). Further reductions in NO_y deposition are expected in coming years resulting from stringent policy actions including the vehicle emission control and the national ambient air quality standards (22).

Regarding NH_x deposition trends (Fig. 4 *A* and *C*), Western Europe was identified as the only region with a continuous decline in recent decades (16%, 1980–2009) due to the agricultural emission reduction measures under the Union Common Agricultural Policy (25), while NH_x deposition increased slightly after 2009 (from 2.0 Tg to 2.2 Tg in 2018). For instance, NH_3 abatement was required in policies of Denmark and Netherlands (15), leading to reduction of NH_x deposition by 40% and 10% between 1990 and 2018 (*SI Appendix*, Fig. S7). In Western Europe, NH_3 emission reduction would be required for all sectors by 2030, with the guidance of European National Emission Ceilings directive (15). Notably, although NH_3 emissions in Western Europe have reduced since 1980, it does not mean that NH_3 emissions for all Western European countries have decreased. For instance, in Spain, NH_x deposition has increased since 1980 (*SI Appendix*, Fig. S7). The 2020 European Environment Agency report also indicated that NH_3 emissions in Spain were 33% above ceiling levels with the highest exceedances for all 27 member states (26). Reducing NH_3 emissions will continue to be a major challenge in Western Europe. Although Western Europe had continuous decreasing NH_x deposition in recent decades, other countries have experienced a rapid increasing trend. For the United States, despite its successful controls in NO_y deposition, its NH_x deposition has increased by 14% from 1980 (2.2 Tg N) to 2019 (2.5 Tg N) because NH_3 emissions in the United States are not strictly regulated. The estimated increasing NH_x deposition in the United States was consistent with an observational study, which found NH_x deposition increased by 10–20% from 1990 to 2010 (22). Compared to Western Europe and the United States, China's NH_x deposition increased greatly by 113% from 1980 (4.7 Tg N) to 2015 (10.0 Tg N). After 2015, China's NH_x deposition became stable with a slight decreasing trend. The stabilization in China's NH_x deposition after 2015 can be also supported by the NNDMN measurements (24), which may be partly explained by the implementation of Zero Increase Action Plan for N fertilizer after 2015. China's NH_x deposition was still much too high (9.4 Tg N in 2018), which was substantially larger (4 times) compared to that in the United States (2.5 Tg N) and Western Europe (2.2 Tg N). *SI Appendix*, Fig. S8 shows regional N_r deposition in China, the United States, and Western Europe expressed by per unit area (kg N ha^{-1} y^{-1}), presenting similar regional trends and differences as indicated by Fig. 4. China's N_r deposition in the 2010s (>15 Tg N) was much larger than those of the United States and Western Europe in 1980s (7–8 Tg N), when the Clean Air Act and emission control had not been fully implemented (11). Challenges faced by China are much higher than those in the United States and Europe. For other developing countries, a similar continuous increasing trend in NH_x deposition since 1980 was also found in India, Pakistan, Mongolia, Brazil, and Sudan (*SI Appendix*, Fig. S9) because no limitation was implemented on NH_3 emissions. For the global totals on land, NH_x deposition increased by 72% from 1980 (25 Tg N) to 2018 (44 Tg N). *SI Appendix*, Fig. S10 shows the time series of the relative contribution of NH_x to total N_r deposition ($R_{NHx/Nr}$) on land globally in China, the United States, and Western Europe. Increasing importance of NH_x to total N_r deposition for the globe can be clearly seen from 0.41 in 1980 to 0.54 in 2018. Similar phenomena with increased $R_{NHx/Nr}$ can be also found for the United States (0.31–0.52) and Western Europe (0.33–0.47). However, for China, the $R_{NHx/Nr}$ first decreased from 0.78 in 1980 to 0.59 in 2011, and then increased after 2011 (0.59–0.65). The decrease of $R_{NHx/Nr}$ in China between 1980 and 2011 was mainly due to the speed of NO_y deposition driven by fossil fuel combustion that exceeded that of NH_x deposition driven by agriculture, while the increased $R_{NHx/Nr}$ after 2011 can be explained by reduction measures for NO_x emissions by the Chinese government. Increasing agricultural NH_3 emissions and the success of control measures in reducing NO_x emissions are changing the temporal patterns of global N_r deposition. NH_x dominated total N_r depositions in most countries in the recent decade and would account for a larger part of total N_r depositions due to the lack of NH_3 regulations.

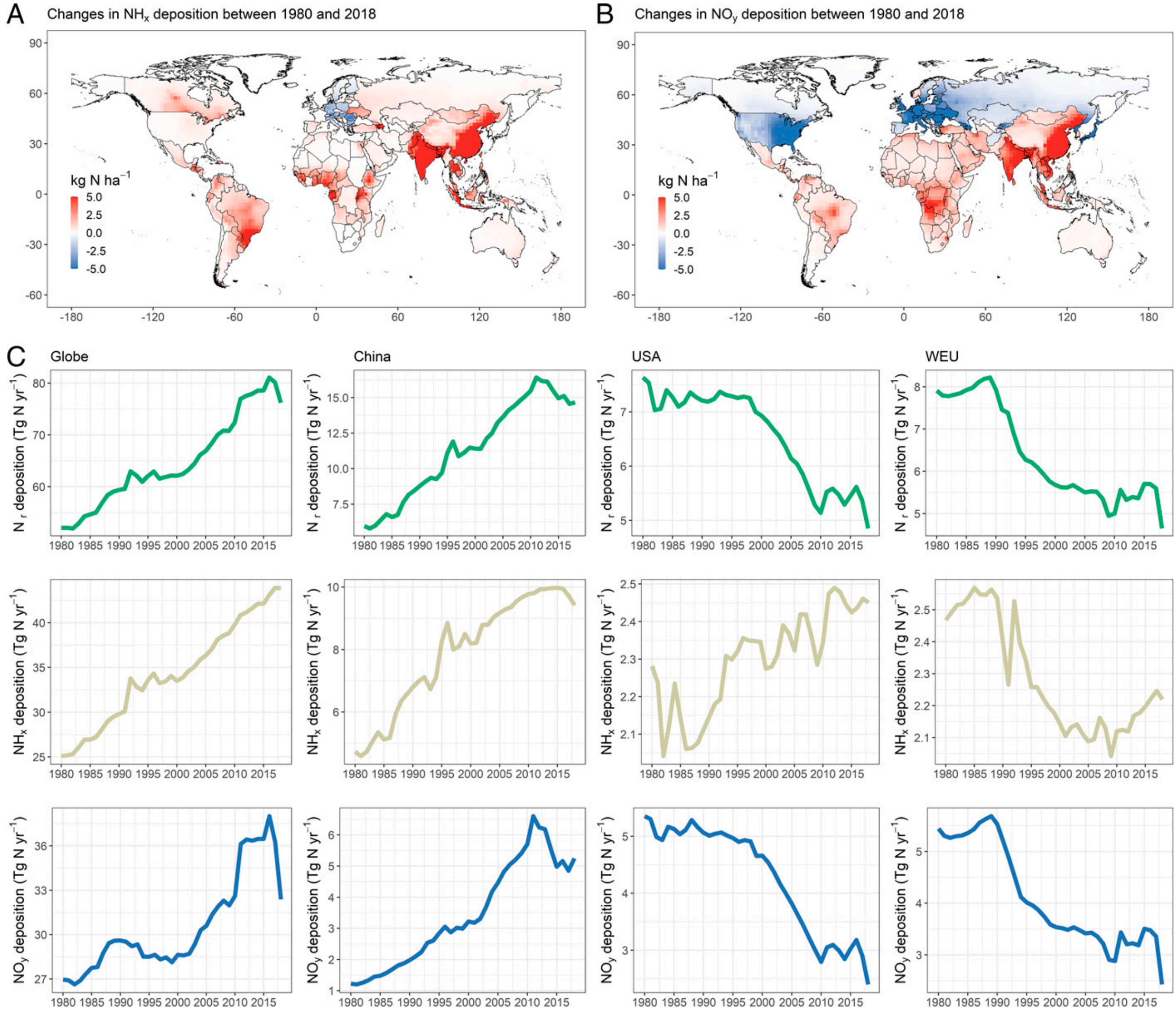

Fig. 4. Changes of N_r deposition. Spatial changes of (*A*) NH_x and (*B*) NO_y deposition between 1980 and 2018. (*C*) Time series of N_r deposition on land globally in China, the United States, and Western Europe.

Discussion and Implications

Global total NH_x deposition increased by 70% in recent four decades due to the lack of policies in reducing agricultural NH_3 pollution worldwide (except Western Europe). We foresee that, without NH_3 emission reduction in the future, NH_x deposition will continue to increase, and occupy a greater dominant position in total N_r deposition. Previous studies pointed to the overuse of N fertilizer as one major contributor to excessive N_r deposition (1, 27). Our developed agricultural NH_3 emissions demonstrated that three crops (rice, wheat, and maize) accounted for 68% of cropland NH_3 emissions. Using a yield-response model (see *Materials and Methods*), 38% of N fertilizer can be reduced without impacting current yields (Fig. 5*C* and *SI Appendix*, Fig. S13 and Table S1), and three crops (rice, wheat and maize) are responsible for 72% of the excessive N fertilizer of the 16 crops globally. For the hotspot regions, China, India, and the United States accounted for 65% of global excessive N fertilizer.

Nitrogen fertilizer overuse accounted for 25% of cropland NH_3 emissions (0–55% by country), and 11% of total NH_3 emissions (cropland plus livestock) (Fig. 5*E*). Regionally, the contribution of N overuse to total NH_3 emissions in China, the United States, and India was 31%, 25%, and 22%, respectively, while it was close to 0 in Africa, Southern America, and Russia because these areas had low N fertilizer. Low-yield performing was found in Africa, South America, and Russia (Fig. 5*D*) with the ratio of the observed to attainable yields below 0.5. Taking wheat, rice, and maize as an example, the ratio of current yields to attainable yields was below 50% over many regions, especially for the Sub-Saharan Africa (Eritrea, 27%; Sudan, 40%; Rwanda, 35%; Congo, 19%), South America (Brazil, 47%) and Russia (38%) (Fig. 5*D* and *SI Appendix*, Fig. S12).

It is still unclear on how much N fertilizer overuse contributes to N_r deposition. We calculated the contribution of potential N fertilizer overuse to N_r deposition using the GEOS-Chem for the base year 2010 as a case study. NH_x deposition induced by N overuse accounted for 17% globally, while the contribution of N overuse to total N_r deposition was 10%. Higher contribution of N overuse to total N_r deposition occurred in China (20%), followed by India (15%), the United States (12%), and Western Europe (10%) (Fig. 4*F*). This suggests that 10 to 20% of total N_r

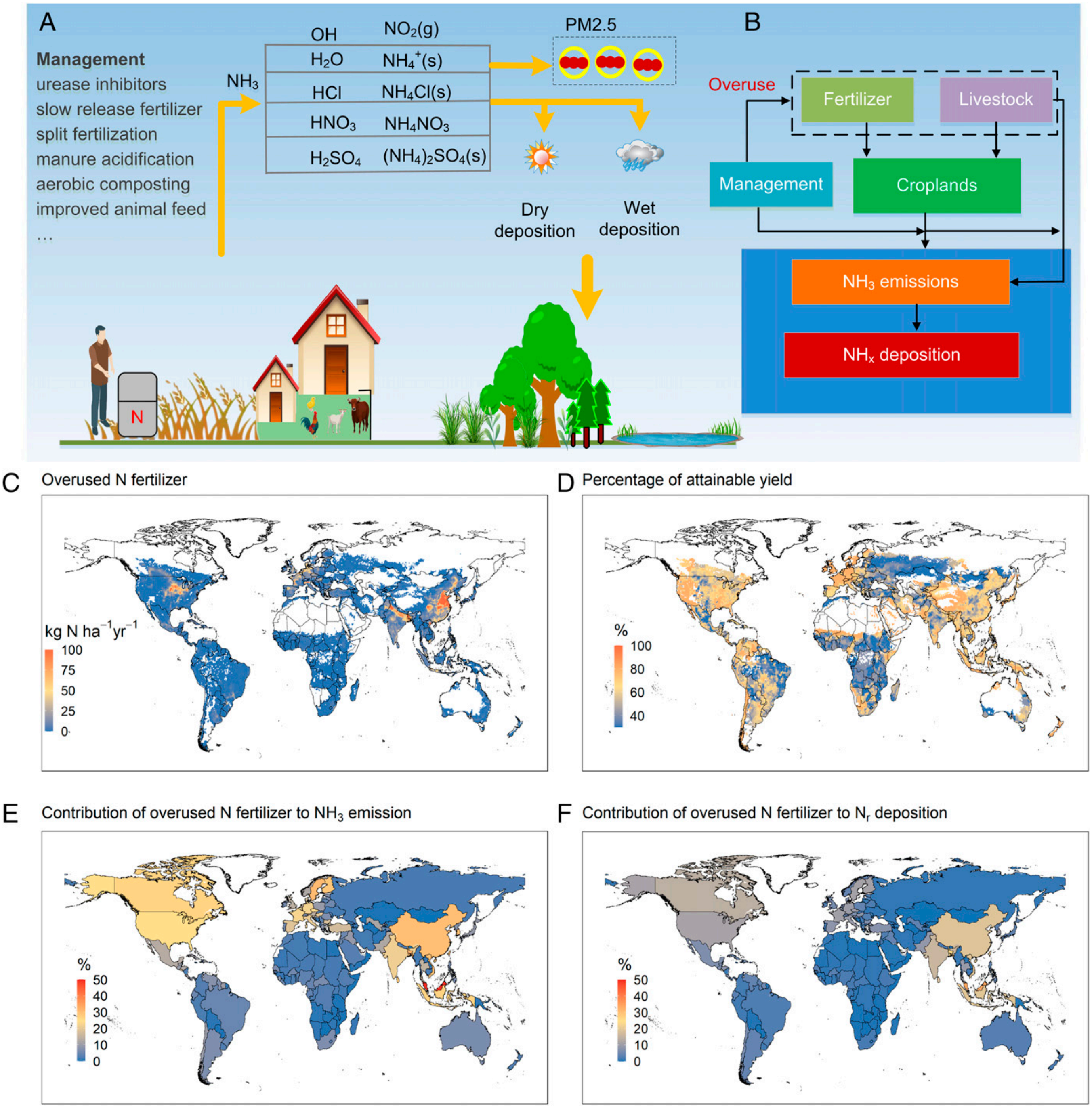

Fig. 5. Contribution of N fertilizer overuse to N_r deposition. (*A*) Schematic illustration of agricultural NH_3 emissions and N_r deposition. (*B*) A flowchart of calculating agricultural NH_3 emissions and N_r deposition. (*C*) Avoidable N application without affecting current yields. N fertilizer overuse by each crop can be found in *SI Appendix*, Fig. S13. (*D*) Average percentage of the attainable yield achieved by wheat, maize, and rice. Spatial maps of the percent attainable yield for each crop can be found in *SI Appendix*, Fig. S12. (*E*) Contribution of N fertilizer overuse to NH_3 emissions. (*F*) Contribution of N fertilizer overuse to N_r deposition by country.

deposition can be reduced if N overuse was avoided in these hotspot areas through appropriate nutrient management. Thus, reducing N overuse for a small number of crops and countries may have a significant impact on global NH_3 emissions.

Although Western European countries (such as Denmark and Netherlands) have adopted the nutrient managements (such as optimizing N fertilizer) along with emission control policies, many other countries (such as China, India, and the United States) still have a long way to address NH_3 pollution in terms of lacking policies regarding reducing N overuse. As the world's highest NH_3 emission region, China began to mitigate agricultural NH_3 emission during the 13th Five Year Plan (2016–2020), and it was estimated that China's NH_3 emission could be reduced by half through nutrient managements and appropriate policies (such as subsidies for reductions of urea-based fertilizer, promotion of enhanced efficiency N fertilizer, and machine deep placement of fertilizer) (25). Such improved nutrient management, for example, will also help reduce the imbalances of N and phosphorus in the North China Plain, the Midwest United States, and the sub-Sahara region (e.g., Kenya) (28).

In addition, NH_3 reduction by avoiding N fertilizer overuse would mitigate PM2.5 (with an aerodynamic diameter smaller than

2.5 μm) pollution at the same time (15). High decrease in PM2.5 concentrations would occur in Eastern China with the reduction ranges of 5 to 10 $\mu g\ m^{-3}$, followed by India, the Eastern United States, Western Europe (0–5 $\mu g\ m^{-3}$) (*SI Appendix*, Fig. S14). The decrease in PM2.5 by reduction in agricultural NH_3 emissions support increased emphasis on nutrient management to address NH_3 environmental challenges. Although reducing the production of N_r and its harmful effects will be a challenge, it is both possible and vital. Our comprehensive analysis shows appropriate agricultural strategies can reduce agricultural NH_3 loss and NH_x deposition at large scales while improving food security at the same time. Our work provides guidance for decision-making that can promote a sustainable food system in the future. Besides cropping systems, more structural measures for livestock production systems could further reduce agricultural NH_3 emissions, such as livestock relocation to enhance manure recycling, manure acidification, aerobic composting, and improved animal feed (25). Agricultural nutrient management by improving the efficiency of N fertilizer application would have co-benefits on air quality, human health, food security, climate mitigation, and biodiversity conservation, helping to solve the global N pollution challenge.

Materials and Methods

Agricultural Data. We collected crop related datasets from the EarthStat geographic datasets and the long-term statistical datasets (1980–2018) from the FAO datasets (https://www.fao.org/faostat/en/) for analysis. The EarthStat is collaboration between the Global Landscapes Initiative at the University of Minnesota's Institute on the Environment and the Land Use and Global Environment laboratory at the University of British Columbia. The FAO collected relevant national statistical information related to food and agriculture including the crop and livestock data. We used the FAO "Fertilizers by Nutrient" data by country between 1980 and 2018 that cover 16 major crops analyzed here. The FAO included N fertilizer input for each crop by country in unit of both kg N $ha^{-1}\ y^{-1}$ and Tg N y^{-1}. We used the FAO statistical data to scale the EarthStat geospatial data by country. We focused our analysis on 16 key crops, composing the 16 highest-calorie-producing crops consumed as food (*SI Appendix*, Table S1). These 16 crops accounted for 60% of the global cropland area harvested and 70% of all N application on croplands and produced 86% of the world's crop calories. N application rate and consumption data were compiled for nations and subnational units across the globe. The crop related subnational data were mainly from statistical bureaus and national-level fertilizer industry associations at the provincial or state levels. Crop-specific application rates were then distributed across detailed maps of crop and pasture areas, and rates were harmonized with subnational and national nutrient consumption data.

We used a new version of the Gridded Livestock of the World (GLW3) database, reflecting the most recently compiled and harmonized subnational livestock distribution data for the year 2010 (https://dataverse.harvard.edu/dataverse/glw_3). GLW3 provides global population densities of cattle, buffalos, horses, sheep, goats, pigs, chickens, and ducks in each land pixel at a spatial resolution of 0.083 decimal degrees. They are accompanied by detailed metadata on the year, spatial resolution and source of the input census data. The FAO included the 8 major animals analyzed in this study in the unit of head in each country since 1980. We have detailed spatial distribution data of each animal in 2010s from the GLW3, while it is still very challenging to obtain animal-specific information at the subnational scales especially in 1980s. For the long-term datasets (1980–2018), we used the FAO statistics of animal number by country to scale the 2010 spatial data and then estimated livestock NH_3 emissions. Our estimated livestock NH_3 emissions are particularly helpful for national comparisons and temporal analysis at the regional scales.

Agricultural NH_3 Emissions between 1980–2018. We developed an agricultural NH_3 emission dataset from N fertilizer and livestock during 1980 to 2018. The NH_3 emission model represented N fertilizer application for 16 crops and livestock for 8 animals. The NH_3 emission model we used was a bottom-up NH_3 emission estimation from both N application and livestock waste using recently published geospatial data (4, 12) and long-term statistics from the FAO of the United Nations. Agricultural NH_3 emissions, from livestock production and cropland planting, were calculated by the bottom-up methods based on activities data and corresponding condition-specific EFs, according to the following equation:

$$E(NH_3) = \sum_t \sum_{ij} A_{tij} \times EF_{tij}, \qquad [1]$$

where $E(NH_3)$ was the total agricultural NH_3 emissions, t represented the source type (including crop-specific N fertilizers and livestock production [head]), i and j represented the grid row and column of global map (0.083° grids), A_{tij} was the activity data of a specific source, and EF_{tij} was the corresponding EFs. Crop groups included rice, wheat, maize, cotton, soybean, sugar crops, roots, oil crops, and other cereals (*SI Appendix*, Table S1). Different livestock mainly focused on 8 significant animals (buffalos, cattle, chickens, ducks, goats, sheep, horses, and pigs). Further details on the estimate methods and gridded allocation of the various sources were presented in previous studies (6, 29). Emission factors of NH_3 from N fertilizer and livestock were obtained from observation-based measurements by regions from cropping and pasture systems. The results were categorized by country, and the average by continent was shown in *SI Appendix*, Table S3 including Asia, Europe, North America, and South America.

N_r Deposition by GEOS-Chem. The GEOS-Chem, a widely used global chemical transport model (v12-03, http://www.geos-chem.org), was applied to simulate long-term N_r deposition (1980–2018). It includes a detailed simulation of tropospheric gas-aerosol chemistry and has been applied in a number of studies to simulate atmospheric N_r deposition. GEOS-Chem parameterizes dry deposition of gases and aerosols by a standard big leaf resistance model and wet deposition separated by the convective updraft and large-scale precipitation scavenging (10, 21). The surface-atmosphere bidirectional NH_3 fluxes are not considered in current deposition model simulations. The long-term MERRA2 assimilated meteorological data from the NASA Global Modeling and Assimilation Office were used to drive GEOS-Chem. The "tropchem" scheme of GEOS-Chem model was run at a horizontal resolution of 2° latitude by 2.5° longitude and 47 levels in the vertical. Spin-up simulation was performed with 6 mo before the actual simulation time for our analysis typically exceeding atmospheric NH_3 lifetime usually within 24 h and NH_4^+ lifetime usually with 1 wk (30). We used 30-min and 15-min time steps for chemistry and transmission, respectively, as set similar to a previous study (31).

For agricultural NH_3 emissions, we used our developed high-resolution dataset, while the anthropogenic NO_x emissions were obtained from the newly updated global CEDS during 1980 to 2014, overwritten by regional inventories including EMEP over Europe and REAS v3 over East Asia, NEI in the United States, and CAC in Canada. For the years 2015 to 2018, we adopted the methods of Geddes et al. (31) to scale the 2014 base emissions to 2015 to 2019 according to the satellite observations (i.e., for NO_x by OMI and NH_3 by IASI). The natural NO_x and NH_3 emissions include GFED biomass burning, lightning, soil, and the biosphere. All emissions were treated with the Harvard emission components (HEMCO) system designed for deriving emissions in atmospheric models.

N Fertilizer Overuse and Its Contribution to NH_3 Emissions. We explored the potential overuse of N fertilizer for 16 major crops. A crop- and climate-specific yield response model was used to calculate the amount of fertilizer application that could be reduced yet still get the same yields. We refer to this potential as avoidable N. The yields for each crop are divided into 100 climate bins of equal harvested area. Bins are crop-specific and are defined based on annual precipitation and growing-degree days (*SI Appendix*, Fig. S11). Notably, we excluded climate outliers and used crop specific equal area climatic zones. Within each climate bin, the yield response model uses Mitscherlich–Baule curves to describe the saturating relationship between yield and additional inputs of N (4, 32):

$$\text{Yield} = \text{Yield}_{max}(1 - b_N * e^{-c_N * \text{Nfer}}), \qquad [2]$$

where Y_{max} is the maximum yield possible within the climate bin; b_N describes the y-intercepts for each nutrient-yield response curve; c_N are response coefficients that describe the percent of Y_{max} achieved at a given nutrient level. Climatic potential yields are defined as the 95th percentile range of yields for a given crop in a given bin.

We then used the model to estimate the required amount of N needed to obtain current yields:

$$\mathrm{Nfer}_{req} = -\ln\left(\frac{1-(Y_{true}/Y_{max})}{b_N}\right)/c_N. \quad [3]$$

Since the model is based on current yields and management practices, this approach estimates best N application rates that minimize excessive N. The model was only used when R^2 is ≥ 0.30 for within-bin variability explained by Mitscherlich–Baule curves.

After estimating avoidable N fertilizer, we applied it to estimate new NH_3 emissions and calculated the contribution of N overuse to total N_r deposition globally using the GEOS-Chem model. The NH_3 emissions caused by N overuse were calculated as:

$$\Delta E_{NH3} = \sum_{ij} \Delta A_{tij} \times EF_{tij}, \quad [4]$$

where ΔE_{NH3} is agricultural NH_3 emissions induced by N overuse, ΔA_{tij} is the overuse N, and EF_{tij} is the original emission factor.

Data Availability. The crop and livestock related dataset and GEOS-Chem model code in this study are publicly available for download. Crop data from the EarthStat can be downloaded from http://www.earthstat.org/nutrient-application-major-crops/. The FAO long-term statistic data can be freely accessed from https://www.fao.org/faostat/en/#data/EF. The livestock data are available from Harvard Dataverse at https://dataverse.harvard.edu/dataverse/glw_3. The GEOS-Chem model code is open source (https://doi.org/10.5281/zenodo.3676008). All other study data are included in the article and/or the supporting information.

ACKNOWLEDGMENTS. This study is supported by the National Natural Science Foundation of China (42001347, 41471343, 41425007, 41705130, and 41922037), the Chinese State Key Research & Development Programme (2017YFC0210100 and 2017YFD0200101), and the High-Level Team Project of China Agricultural University (to X.L.). The analysis in this study is supported by the Supercomputing Center of Lanzhou University.

Author affiliations: [a]College of Earth and Environmental Sciences, Lanzhou University, Lanzhou 730000, China; [b]Key Laboratory of Plant-Soil Interactions of Ministry of Education (MOE), Beijing Key Laboratory of Farmland Soil Pollution Prevention and Remediation, College of Resources and Environmental Sciences, National Academy of Agriculture Green Development, China Agricultural University, Beijing 100193, China; [c]Key Laboratory of Vegetation Restoration and Management of Degraded Ecosystems, South China Botanical Garden, Chinese Academy of Sciences, Guangzhou 510650, China; [d]Laboratory for Climate and Ocean-Atmosphere Studies, Department of Atmospheric and Oceanic Sciences, School of Physics, Peking University, Beijing 100871, China; [e]School of Atmospheric Sciences, Sun Yat-sen University, Zhuhai 510275, China; [f]College of Oceanic and Atmospheric Sciences, Ocean University of China, Qingdao 266100, China; [g]International Institute for Earth System Science, Nanjing University, Nanjing 210023, China; [h]Key Laboratory of Crop Physiology and Ecology in Southern China, Nanjing Agricultural University, Nanjing, 210095, China; and [i]Department of Biology, Stanford University, Stanford, CA 94016

1. X. Liu *et al.*, Enhanced nitrogen deposition over China. *Nature* **494**, 459–462 (2013).
2. J. N. Galloway *et al.*, Transformation of the nitrogen cycle: Recent trends, questions, and potential solutions. *Science* **320**, 889–892 (2008).
3. D. E. Canfield, A. N. Glazer, P. G. Falkowski, The evolution and future of Earth's nitrogen cycle. *Science* **330**, 192–196 (2010).
4. N. D. Mueller *et al.*, Closing yield gaps through nutrient and water management. *Nature* **490**, 254–257 (2012).
5. Y. Guo *et al.*, Air quality, nitrogen use efficiency and food security in China are improved by cost-effective agricultural nitrogen management. *Nat. Food* **1**, 648–658 (2020).
6. M. Liu *et al.*, Ammonia emission control in China would mitigate haze pollution and nitrogen deposition, but worsen acid rain. *Proc. Natl. Acad. Sci. U.S.A.* **116**, 7760–7765 (2019).
7. L. Lassaletta, G. Billen, B. Grizzetti, J. Anglade, J. Garnier, 50 year trends in nitrogen use efficiency of world cropping systems: The relationship between yield and nitrogen input to cropland. *Environ. Res. Lett.* **9**, 105011 (2014).
8. X. Zhang *et al.*, Societal benefits of halving agricultural ammonia emissions in China far exceed the abatement costs. *Nat. Commun.* **11**, 4357 (2020).
9. L. Zhang *et al.*, Agricultural ammonia emissions in China: Reconciling bottom-up and top-down estimates. *Atmos. Chem. Phys.* **18**, 339–355 (2018).
10. L. Zhang *et al.*, Nitrogen deposition to the United States: Distribution, sources, and processes. *Atmos. Chem. Phys.* **12**, 4539–4554 (2012).
11. B. Gu, X. Ju, J. Chang, Y. Ge, P. M. Vitousek, Integrated reactive nitrogen budgets and future trends in China. *Proc. Natl. Acad. Sci. U.S.A.* **112**, 8792–8797 (2015).
12. M. Gilbert *et al.*, Global distribution data for cattle, buffaloes, horses, sheep, goats, pigs, chickens and ducks in 2010. *Sci. Data* **5**, 180227 (2018).
13. H. Cao *et al.*, Inverse modeling of NH_3 sources using CrIS remote sensing measurements. *Environ. Res. Lett.* **15**, 104082 (2020).
14. European Environment Agency, European Union Emission Inventory Report 1990-2018 (2018).
15. B. Gu *et al.*, Abating ammonia is more cost-effective than nitrogen oxides for mitigating PM2.5 air pollution. *Science* **374**, 758–762 (2021).
16. P. Ruyssenaars, J. P. Hettelingh, F. D. Leeuw, M. Posch, A. Lukewille, Evaluation of progress under the EU National Emissions Ceilings Directive (European Environment Agency, 2012).
17. R. M. Hoesly *et al.*, Historical (1750–2014) anthropogenic emissions of reactive gases and aerosols from the Community Emissions Data System (CEDS). *Geosci. Model Dev.* **11**, 369–408 (2018).
18. X. Zhang *et al.*, Ammonia emissions may be substantially underestimated in China. *Environ. Sci. Technol.* **51**, 12089–12096 (2017).
19. L. Liu *et al.*, Temporal characteristics of atmospheric ammonia and nitrogen dioxide over China based on emission data, satellite observations and atmospheric transport modeling since 1980. *Atmos. Chem. Phys.* **17**, 1–32 (2017).
20. J. Tan *et al.*, Multi-model study of HTAP II on sulfur and nitrogen deposition. *Atmos. Chem. Phys.* **18**, 1–36 (2018).
21. Y. Zhao *et al.*, Atmospheric nitrogen deposition to China: A model analysis on nitrogen budget and critical load exceedance. *Atmos. Environ.* **153**, 32–40 (2017).
22. Y. Li *et al.*, Increasing importance of deposition of reduced nitrogen in the United States. *Proc. Natl. Acad. Sci. U.S.A.* **113**, 5874–5879 (2016).
23. Q. Zhang *et al.*, NO_x emission trends for China, 1995-2004: The view from the ground and the view from space. *J. Geophys. Res. Atmos.* **112**, 1–18 (2007).
24. Z. Wen *et al.*, Changes of nitrogen deposition in China from 1980 to 2018. *Environ. Int.* **144**, 106022 (2020).
25. L. Liu *et al.*, Challenges for global sustainable nitrogen management in agricultural systems. *J. Agric. Food Chem.* **68**, 3354–3361 (2020).
26. EEA, National Emission Reduction Commitments Directive reporting status 2020 (European Environment Agency, 2020). https://www.eea.europa.eu/publications/national-emission-reduction-commitments-directive
27. X. Liu *et al.*, Nitrogen deposition and its ecological impact in China: An overview. *Environ. Pollut.* **159**, 2251–2264 (2011).
28. P. M. Vitousek *et al.*, Agriculture. Nutrient imbalances in agricultural development. *Science* **324**, 1519–1520 (2009).
29. Y. Kang *et al.*, High-resolution ammonia emissions inventories in China from 1980 to 2012. *Atmos. Chem. Phys.* **16**, 2043–2058 (2016).
30. M. Van Damme *et al.*, Industrial and agricultural ammonia point sources exposed. *Nature* **564**, 99–103 (2018).
31. J. A. Geddes, R. V. Martin, Global deposition of total reactive nitrogen oxides from 1996 to 2014 constrained with satellite observations of NO_2 columns. *Atmos. Chem. Phys.* **17**, 10071–10091 (2017).
32. P. C. West *et al.*, Leverage points for improving global food security and the environment. *Science* **345**, 325–328 (2014).